

## Universal spectral structure in pendulum-like systems

Teepanis Chachiyo<sup>a)</sup>

*Department of Physics, Faculty of Science, Naresuan University, Phitsanulok 65000, Thailand*

(Dated: 6 March 2026)

Pendulum-like dynamics is a universal motif across many areas of physics, underlying systems ranging from classical nonlinear oscillators to superconducting circuits and tunneling dynamics in cold-atom platforms. Here we present an exact frequency-domain formulation of the pendulum equation that applies uniformly across oscillatory, separatrix, and rotational regimes. The resulting spectral representation reveals a previously hidden unification: all regimes share the same analytic spectral structure and characteristic frequency scale. We show that oscillatory, stopping, and rotational regimes all arise from a single universal spectral kernel, with parity selection distinguishing the periodic motions and the separatrix representing their discrete-to-continuum limit. Regime changes thus correspond to symmetry-driven reorganizations in frequency space rather than changes in the underlying spectral structure, with the stopping trajectory representing the continuum limit reached without system-size scaling. The spectral structure can be derived via a spectral discretization approach starting from the separatrix solution, without relying on the classical Jacobi elliptic formulation. Beyond providing closed-form solutions, the framework reveals a transparent spectral structure underlying a broad class of classical and quantum pendulum-like systems.

Keywords: nonlinear dynamics; separatrix; regime transitions; spectral structure; frequency-domain analysis; superconducting circuits; cold-atom systems

---

<sup>a)</sup>Electronic mail: teepanisc@nu.ac.th

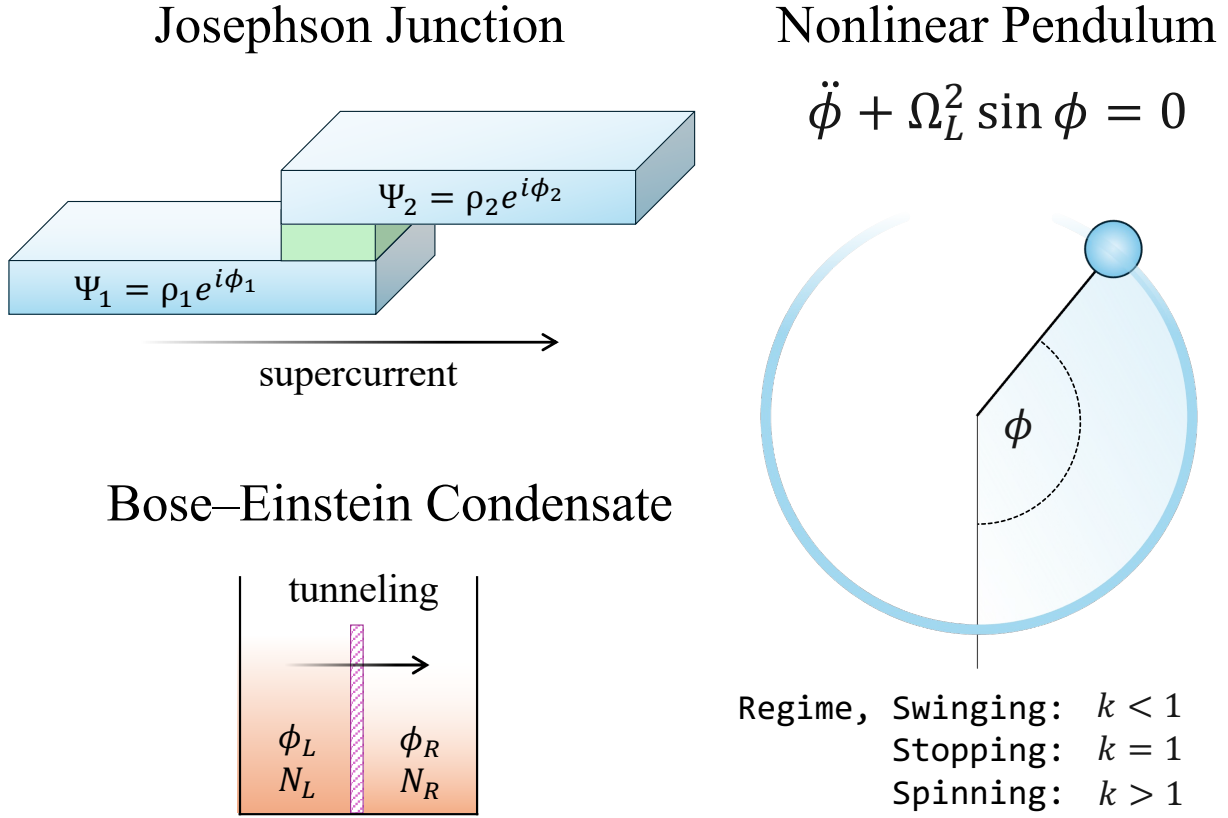


FIG. 1. **Pendulum-like dynamics across classical and quantum systems.** (a) Superconducting Josephson junction, where the phase difference  $\phi = \phi_2 - \phi_1$  governs the supercurrent. (b) Neutral-atom (bosonic) Josephson junction with populations  $N_L$  and  $N_R$  and tunneling between condensates. (c) Nonlinear pendulum with angular displacement  $\varphi$ . All systems are described by the nonlinear phase equation  $\ddot{\phi} + \Omega_L^2 \sin \phi = 0$ , which admits swinging, stopping, and spinning regimes.

## I. INTRODUCTION

Pendulum-like dynamics, as shown in Fig. 1, remains an active topic of research<sup>1–5</sup>, with broad applications ranging from superconducting Josephson junctions<sup>6,7</sup> and Bose–Einstein condensate tunneling<sup>8,9</sup> to energy harvesting and artificial intelligence<sup>10–13</sup>. For example, pendulum-based mechanisms can harvest energy from human motion<sup>11</sup> or ocean waves via piezoelectric coupling<sup>12</sup>, while machine-learning models employ analytical pendulum solutions to recognize continuous nonlinear dynamics<sup>13</sup>.

Energy-conserving pendulum-like dynamics are governed by the following equation:

$$\frac{d^2}{dt^2}\phi(t) + \Omega_L^2 \sin \phi = 0. \quad (1)$$

Here,  $\phi(t)$  and  $\Omega_L$  are the characteristic dynamical phase and the angular frequency of *linear* oscillation.  $\Omega_L^2$  depends on physical parameters of the system. For example,  $\Omega_L^2 = g/L$  in a classical pendulum<sup>14–16</sup>,  $2eI_c/(\hbar C)$  in an ideal Josephson junction<sup>17</sup>, or  $[\frac{2J}{\hbar}\sqrt{\Lambda + \lambda}]^2$  in Bose–Einstein condensate tunneling<sup>9</sup>.

Because these systems are intrinsically oscillatory, exact frequency-domain solutions of pendulum-like dynamics could further advance their development across diverse fields. However, despite its long history dating back to Galileo<sup>18</sup> and the foundational work of Euler and Jacobi, the nonlinear pendulum remains analytically incomplete in the frequency domain. While exact time-domain solutions exist in terms of Jacobi elliptic functions<sup>19,20</sup>, their nested form obscures the spectral content of the motion. For example, the time-domain solution involves a Jacobi elliptic sine function,  $\text{sn}(z, k)$ . It is true that an exact Fourier series of  $\text{sn}(z, k)$  is known<sup>21</sup> (22.11.E1). However, the form of the exact  $\phi(t)$  is such that the Jacobi elliptic sine is wrapped inside an arcsine function,  $\phi(t) = 2 \arcsin[k \text{sn}(\Omega_L t + K, k)]$ <sup>19,22</sup>. Unless a clever mathematical manipulation is performed to unwrap it, knowing the exact Fourier series of  $\text{sn}(z, k)$  does not constitute an exact Fourier series of  $\phi(t)$ .

As a result, studies of the nonlinear pendulum have relied on numerical methods<sup>23,24</sup> or sophisticated theoretical schemes<sup>25–27</sup> to compute the Fourier coefficients of  $\phi(t)$ , with increasingly complicated expressions for higher harmonics. The Fourier series for a pendulum with large amplitudes has also been revisited<sup>28,29</sup>. These studies meticulously confirm through experimental measurements that the motion indeed consists of odd harmonics. However, the theoretical Fourier coefficients are obtained from a perturbation method, in which  $\sin \phi$  is replaced by a power series<sup>30,31</sup>. Harmonics then appear in the solution for each order of the perturbation. Collecting and regrouping the harmonics result in the Fourier coefficients being expressed as a power series in the amplitude,  $\phi_0$ . The series is truncated because the equation for each order of the perturbation becomes increasingly complex. Therefore, the Fourier coefficients are practically an approximation.

The absence of an exact closed-form expression for the Fourier coefficients underscores that frequency-domain analysis of the nonlinear pendulum has remained unresolved for centuries. Previous approaches have yielded only approximate or numerical results, limited to

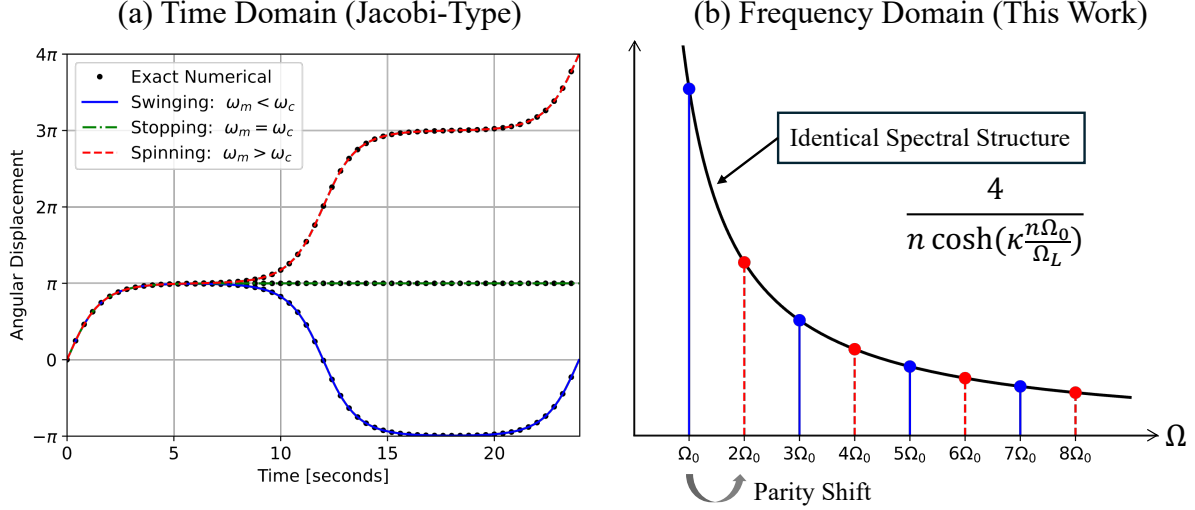


FIG. 2. **Time- and frequency-domain representations of pendulum-like dynamics.** (a)  $\phi(t)$  for swinging ( $\omega_m = \omega_c - 10^{-4}$ ), stopping ( $\omega_m = \omega_c$ ), and spinning ( $\omega_m = \omega_c + 10^{-4}$ ) motions, comparing the spectral solutions in Eqs. (3)–(6) with exact numerical results obtained from Jacobi elliptic functions. (b) Corresponding frequency-domain representation, showing that all three regimes share the same analytic spectral structure, while differing only by parity selection of harmonics (odd for swinging, even for spinning) and by a discrete-to-continuum transition at the separatrix.

specific regimes or initial conditions. Here, we present complete and exact frequency-domain solutions for all three classes of motion—swinging, stopping, and spinning—establishing a unified analytic framework that resolves this long-standing problem.

## II. FORMALISM

Nonlinear motions of an energy-conserving pendulum can be divided into three classes: Swinging, Stopping, and Spinning. These names are coined in this work to enhance intuitive interpretation. Consider the case where the pendulum starts at the bottom,  $\phi_0 = 0$ , with only  $\omega_0$  to initiate the motion. Due to conservation of energy, the angular speed at the bottom is always maximal; thus,  $\omega_m$  will be used to denote the angular speed at the bottom.

If  $\omega_m$  that initiates the motion is too low, the pendulum will not reach the top and will inevitably fall back down. This is referred to as “Swinging” motion. If  $\omega_m$  is just sufficient

for the pendulum to reach the top, it will approach the top but never quite get there. This is because conservation of energy dictates that the closer the pendulum gets to the top, the slower it moves. Ideally and conceptually, the pendulum approaches the top asymptotically, and the angular speed decreases exponentially in time. This is referred to as “Stopping” motion. Finally, if  $\omega_m$  is too large, the pendulum will continue to rotate in one direction. This is referred to as “Spinning” motion.

There exists a critical value of angular speed,  $\omega_c$ , which separates the motion into three distinct classes. Using conservation of energy, it is straightforward to show that

$$\omega_c = 2\Omega_L, \quad k \equiv \frac{\omega_m}{\omega_c} \begin{cases} k < 1 & \text{swinging} \\ k = 1 & \text{stopping} \\ k > 1 & \text{spinning} \end{cases} \quad (2)$$

We now present the exact and unified frequency-domain formulation of the energy-conserving nonlinear pendulum:

$$\text{swinging:} \quad \phi(t) = \sum_{n \text{ odd}} c_n \sin(n\Omega_0 t), \quad (3)$$

$$\text{stopping:} \quad \phi(t) = 2 \arcsin[\tanh(\Omega_L t)], \quad (4)$$

$$\phi(t) = \int_0^\infty d\Omega C(\Omega) \sin(\Omega t), \quad (5)$$

$$\text{spinning:} \quad \phi(t) = 2\Omega_0 t + \sum_{n \text{ even}} c_n \sin(n\Omega_0 t). \quad (6)$$

For simplicity, a closed-form solution for the stopping motion is shown in Eq. (4). For uniformity, however, an integral form can also be written as Eq. (5). In this form, all three classes of motion are now on the same footing, using the frequency domain.

The spectral coefficients  $\{c_n, C(\Omega)\}$  are:

$$\text{swinging, spinning:} \quad c_n = \frac{4}{n \cosh(\kappa \frac{n\Omega_0}{\Omega_L})}, \quad (7)$$

$$\text{stopping:} \quad C(\Omega) = \frac{2}{\Omega \cosh(\kappa \frac{\Omega}{\Omega_L})}, \quad (8)$$

with the parameters  $\kappa$ , fundamental frequency  $\Omega_0$ , and period  $T$  defined uniformly across all regimes as follows:

$$\kappa \equiv K(\sqrt{1-k^2}), \quad \Omega_0 = \frac{2\pi}{T}, \quad T \equiv \frac{4\Re[K(k)]}{\Omega_L}. \quad (9)$$

Here,  $K(k)$  is the complete elliptic integral of the first kind<sup>21,32</sup>. Formally,  $\kappa$  and  $\Omega_0$  remain well-defined positive real quantities for the full range of modulus  $k$ , so that the definitions above apply to all classes of motion.

### III. VALIDATION

Figure 2(a) shows examples of  $\phi(t)$  from this work. As clearly seen, the pendulum starts at the bottom and continues to rise up, but eventually branches off into three distinctive patterns. Quantitatively, the exact numerical values obtained using solutions in the form of Jacobi elliptic functions are also plotted in Fig. 2(a). The agreement is found to be within 14 significant digits, a typical limit of computer precision. Therefore, the solutions in this work are also exact. In addition, the spectral formalism presented here can be readily extended to arbitrary initial conditions by introducing a phase-shift parameter  $\delta$ , which shifts the time origin forward or backward (see Supplementary Material).

Traditionally, the perturbation method has been the primary theoretical tool for studying the frequency content of the nonlinear pendulum<sup>30,31</sup>. However, its scope has been limited to a swinging motion where the pendulum is initially at rest, positioned at an amplitude  $\phi_0$ . As a result, the  $\phi(t)$  is often written as a Fourier series of odd harmonics in the perturbation methods. For example, the recent experimental study<sup>29</sup> has used the following coefficients:

$$\begin{aligned} A_1 &= + \left( \phi_0 + \frac{1}{192}\phi_0^3 + \frac{17}{120 \cdot 512}\phi_0^5 + \dots \right) \\ A_3 &= - \left( \frac{1}{192}\phi_0^3 + \frac{1}{6 \cdot 512}\phi_0^5 + \dots \right) \\ A_5 &= + \left( \frac{1}{40 \cdot 512}\phi_0^5 + \dots \right) \end{aligned} \quad (10)$$

Here,  $\{A_1, A_3, A_5\}$  are the coefficients of the odd harmonics. They are power series in the amplitude,  $\phi_0$ , and are shown up to order 5. In general, higher orders are possible but, as previously noted, the expression would be increasingly more complex.

More broadly, the perturbation method offers a versatile mathematical structure that is applicable beyond the energy-conserving pendulum in this study. Therefore, the method is still an invaluable theoretical tool for a wide range of nonlinear dynamics. However, it is

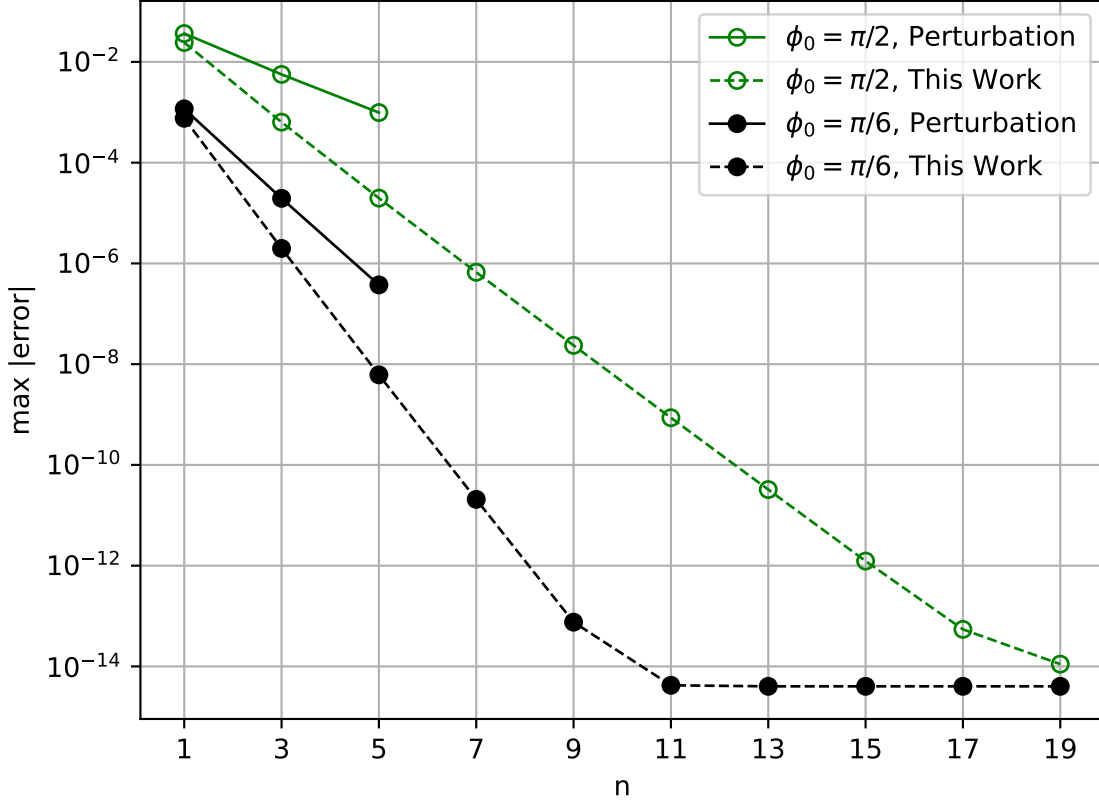


FIG. 3. **Convergence of frequency-domain solutions.** Maximum error of the angular displacement  $\phi(t)$  relative to exact numerical solutions, comparing the perturbation method with the exact spectral solution presented in this work. Results are shown for two initial amplitudes:  $\phi_0 = \pi/6$  (solid circles) and  $\phi_0 = \pi/2$  (open circles). The horizontal axis denotes the perturbation order  $n$  for the perturbative approach, or equivalently the number of harmonics retained in the spectral solution. Both methods exhibit exponential convergence, but the closed-form coefficients in Eq. (7) achieve machine precision with fewer harmonics, particularly at larger amplitudes.

instructive to compare the performance of the frequency content given by the perturbation method and that of Eq. (7) in this work.

Figure 3 shows the maximum error of  $\phi(t)$  from the perturbation method relative to the exact numerical solutions. Two amplitude cases are presented: small amplitude  $\phi_0 = \pi/6$  (solid circle) and large amplitude  $\phi_0 = \pi/2$  (open circle). The horizontal axis indicates the order of the perturbation, with available values  $n = 1, 3, 5$ . The graph also shows the

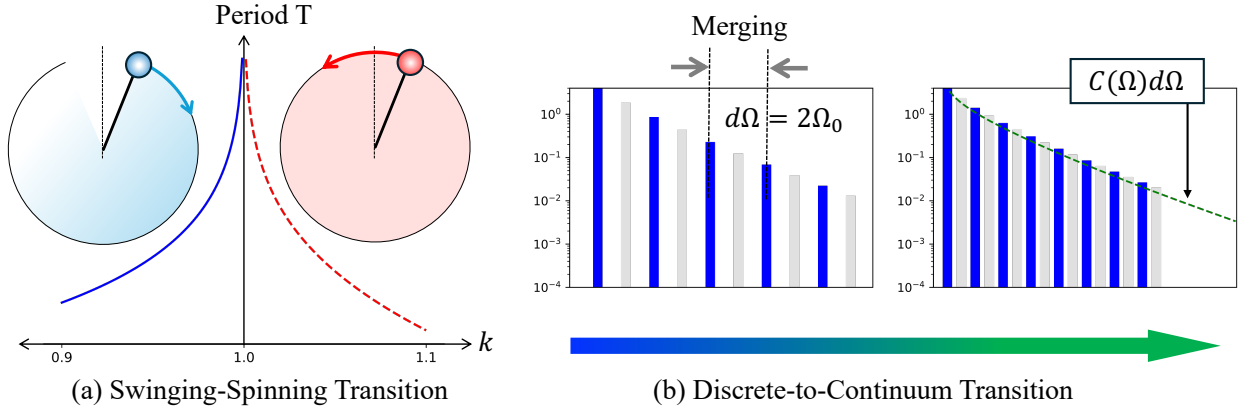


FIG. 4. **Transition between regimes.**

maximum error of  $\phi(t)$  in this work as a function of the number of included harmonics. Together, these graphs provide a comparative view of the convergence performance between the perturbation method and the solution presented in this work.

Both methods exhibit rapid exponential convergence, as indicated by the straight line on the logarithmic scale. Exponential convergence is a desirable feature, particularly given that many periodic functions—such as the square wave—exhibit only polynomial convergence. As expected, better performance is observed at smaller amplitudes, as indicated by the steeper decline in the error. However, the swinging solution in Eq. (3) appears to converge faster as the number of harmonics increases. For the amplitude  $\phi_0 = \pi/6$ , it takes 11 harmonics for the error to reach machine precision. Larger amplitudes require more harmonics, but the coefficients  $a_n$  are already given in closed form and can always be evaluated to the desired precision.

Taken together, the results presented here establish a unified, exact, and frequency-domain description of all regimes of the nonlinear pendulum—swinging, stopping, and spinning. The derived expressions reproduce the time-domain solutions to within machine precision while offering direct access to the spectral structure of the motion through simple elementary functions. Their convergence properties outperform traditional perturbation approaches, which require increasingly complex higher-order expansions to achieve comparable accuracy.

## IV. DISCUSSION

Beyond classical physics, non-intuitive applications of the nonlinear pendulum are found in emerging fields of quantum physics, such as the superconducting Josephson junction<sup>6,7</sup> and, most recently, Bose–Einstein condensate tunneling<sup>8,9</sup>. Despite being fundamentally different physical phenomena, the dynamical models for these examples share the same mathematical structure as the nonlinear pendulum. Therefore, it is useful to discuss the similar physical characteristics that lead to the pendulum-like dynamics, in the context of the formalism of this work. Recognizing these similarities may inspire further applications in quantum physics that share pendulum-like dynamics. The correspondence between the nonlinear pendulum and its quantum analogues is schematically illustrated in Fig. 1, which depict the Josephson junction and the bosonic Josephson junction as physical realizations of pendulum-like phase dynamics.

### A. Quantum Analogues

For example, a Josephson junction (JJ) is a device consisting of two superconducting islands separated by a thin barrier, which can be a normal metal, a narrow superconducting wire, or a thin insulator<sup>33</sup>. Unlike a capacitor (C) or an inductor (L), which are linear electronic devices, the Josephson junction is nonlinear. JJs have been used extensively to construct qubits<sup>33–35</sup>, the fundamental units of quantum computers, in devices like IBM’s quantum processors<sup>36</sup>, Google’s Sycamore Processor<sup>37</sup>, and Zuchongzhi processors<sup>38</sup>.

The dynamics of a Josephson junction can be understood via BCS theory<sup>39</sup>, in which Cooper pairs exist on both superconducting islands. The number of pairs on each island need not be equal, leading to an imbalance of quantum particles between the two sides of the junction. This imbalance can change over time through the tunneling process. Since Cooper pairs are charged particles, their tunneling generates an electric current; likewise, the imbalance gives rise to an electric voltage.

An important quantum mechanical parameter is the phase difference  $\phi$  between the wavefunctions of the two superconducting islands. This is directly analogous to the angle  $\phi$  in the classical pendulum. Following standard circuit theory, the dynamical equation for an ideal Josephson junction (JJ) can be written as<sup>17,40</sup>:

$$\frac{d^2}{dt^2}\phi(t) + \frac{2eI_c}{\hbar C} \sin(\phi) = 0 \quad (11)$$

Here,  $C$  is the stray capacitance due to the junction's geometrical arrangement, and  $I_c$  is the critical tunneling current, which depends on the material, thickness, and area of the junction. As the phase difference  $\phi$  fluctuates—analogueous to the dynamics of the angle  $\phi$  in the pendulum—so do the current through and the voltage across the junction. The current and the voltage are related to wavefunctions phase difference as follows.

$$I = I_c \sin \phi, \quad V = \frac{\hbar}{2e} \frac{d\phi}{dt} \quad (12)$$

In particular, the voltage across the junction plays similar role as the angular velocity of the nonlinear pendulum. In the context of the formalism presented in this work, the dynamics of the ideal Josephson junction can be deduced as follows.

Consider the initial condition where the phase difference is  $\phi = 0$ , and the dynamics are initiated solely by an imbalance of negatively charged Cooper pairs between the two islands. This initial imbalance can also be interpreted as an initial voltage  $V_m$  across the junction. The value of  $V_m$  determines the regime of the dynamics. If  $V_m$  is too low, the voltage simply fluctuates around a zero average. This behavior is analogueous to the swinging motion of a pendulum, where the angular velocity  $\omega(t)$  oscillates back and forth with zero mean.

There exists a critical voltage  $V_c$  that separates the dynamics into three regimes, analogueous to the critical angular velocity  $\omega_c$  defined earlier. If  $V_m = V_c$ , the voltage no longer fluctuates but instead decays toward zero. This corresponds to the separatrix (stopping) regime, where the angular velocity  $\omega(t)$  also decays to zero. If  $V_m > V_c$ , voltage fluctuations resume, but with a non-zero average. This corresponds to the spinning motion of the pendulum, where  $\omega(t)$  oscillates with a non-zero mean. The average voltage across the junction that persists over time can be precisely determined, analogueous to the mean angular velocity  $\bar{\omega}(t) = \Omega_0$  in the spinning solution.

In summary, a Josephson junction is a superconducting device that exhibits a time-varying voltage across the junction, analogueous to the changing angular velocity of a pendulum. The behavior of this voltage can be categorized into three distinct regimes: fluctuations around a zero average, continuous decay toward zero, and fluctuations with a persistent non-zero average.

Another example of a quantum mechanical analogue involves two coupled Bose–Einstein condensates (BECs) of neutral bosonic atoms trapped in a double-well potential, known as a bosonic Josephson junction (BJJ)<sup>41–44</sup>. The bosons can tunnel between the wells, and the key observable variables are the atom number imbalance and the relative phase between the two condensates. The dynamics of the BJJ, modeled as a pendulum, have been extensively studied in the notable work of Pigneur and Schmiedmayer<sup>9</sup>. Their analysis will be briefly revisited here to highlight its similarity to the JJ system.

Unlike Cooper pairs in JJ, the bosons in BJJ are neutral; thus, the imbalance between the two sites does not give rise to the electric voltage. Therefore, the normalized atom number imbalance  $n$ , and the phase difference  $\phi$  are the key conjugating variables describing the dynamics.

$$n = \frac{N_L - N_R}{N_L + N_R}, \quad \phi = \phi_L - \phi_R \quad (13)$$

When the imbalance is appreciably small,  $n(t) \ll 1$ , the dynamical equation can be written as:

$$\frac{d^2}{dt^2}\phi(t) + \left[\frac{2J}{\hbar}\sqrt{\Lambda + \lambda}\right]^2 \sin(\phi) = 0 \quad (14)$$

Here,  $\{J, \Lambda, \lambda\}$  are physical constants characterizing tunneling energy and inter-atomic interaction. Similar to JJ, where the voltage plays the role of angular velocity in classical pendulum,  $n(t)$  in BJJ is related to the phase difference as follow.

$$n(t) = \frac{\hbar}{2J} \frac{1}{\Lambda + \lambda} \frac{d\phi}{dt} \quad (15)$$

Therefore,  $n(t)$  is analogous to  $\omega(t)$  in classical pendulum. As expected, the imbalance  $n(t)$  can vary over time in three distinctive regimes: fluctuations around a zero average, continuous decay toward zero, and fluctuations with a persistent non-zero average.

Having discussed the specific examples of the JJ and BJJ, we can extract general features that give rise to pendulum-like dynamics in quantum systems. First, the system consists of two weakly coupled quantum compartments, with the phase difference  $\phi$  between the wavefunctions in each compartment serving as the key dynamical variable. Second, the weak coupling permits quantum particles to tunnel between compartments, leading to a time-dependent imbalance in particle number. Third, it is energetically favorable for the

system to remain in phase; that is, the potential energy is minimized when  $\phi = 0$ . These three features may give rise to pendulum-like dynamics, as exemplified by the JJ and BJJ systems—cases in which the solutions presented in this work offer a unified and analytically tractable framework for their description.

## B. Symmetry and Transitions Across Regimes

The exact spectral solutions reveal several structural features of pendulum-like dynamics that are not evident in the conventional time-domain formulation. In particular, three key aspects emerge from the frequency-domain perspective and together clarify the symmetry structure and dynamical connectivity of the swinging, stopping, and spinning regimes.

i) *Parity selection in the spectrum.* Figure 2(b) reveals that the distinction between swinging and spinning dynamics is encoded entirely in the parity structure of the frequency spectrum. Swinging motion occupies odd harmonics, while spinning occupies even harmonics with a linear phase drift. Crucially, aside from this parity selection rule, the two regimes share the same spectral structure: the harmonic amplitudes are governed by an identical functional form,

$$c_n = \frac{4}{n \cosh\left(\kappa \frac{n\Omega_0}{\Omega_L}\right)}. \quad (16)$$

In this sense, parity emerges as the organizing principle in frequency space: swinging and spinning are spectrally identical, distinguished solely by parity selection.

ii) *Swinging–spinning regime transition.* Figure 4(a) illustrates a central and nontrivial consequence of the exact spectral solutions: the transition between swinging and spinning dynamics occurs without any change in the fundamental spectral scale. As the system approaches the separatrix from either side, the period of motion diverges logarithmically with identical asymptotic behavior. In dimensionless time units,

$$T_{\text{swing}} \sim T_{\text{spin}} \sim 4 \ln\left(\frac{4}{\sqrt{\delta\omega}}\right), \quad (17)$$

where  $\delta\omega = |\omega_m - \omega_c|$  measures the distance from the critical point. As a result, the fundamental frequency  $\Omega_0 = 2\pi/T$  vanishes in the same manner for both regimes, and the spectral decay scale  $\kappa$  is preserved across the transition. This shows that the swinging–spinning transition is driven by a redistribution of spectral weight, while the underlying frequency structure remains unchanged.

iii) *Discrete-to-continuum transition.* Figure 4(b) highlights a discrete-to-continuum transition that is fundamentally different from those encountered in most areas of physics. In essentially all familiar examples, the emergence of a continuous spectrum is driven by an external thermodynamic or spatial limit. For phonons or photons, discrete modes become continuous only as the size of the confining cavity grows without bound. In electronic systems, discrete molecular energy levels evolve into continuous bands as the number of unit cells increases toward the bulk limit. Similarly, in quantum wells, bound states merge into a continuum as the spatial confinement is weakened or the system size expands. In each case, the continuum arises because the system itself is enlarged and acquires infinitely many degrees of freedom.

The pendulum-like dynamics studied here depart sharply from this paradigm. The system size is fixed, no additional degrees of freedom are introduced, and no spatial or thermodynamic limit is taken. Yet, as the separatrix is approached, the frequency spectrum becomes continuous while preserving the same spectral structure. This discrete-to-continuum transition is therefore not a consequence of system size, geometry, or dimensionality, but is instead generated purely by the nonlinear dynamics of a single degree of freedom.

This distinction is difficult to recognize in the time domain, where the stopping motion appears as a singular trajectory and the separatrix is often treated as a pathological boundary between qualitatively different behaviors. Only through the exact frequency-domain formulation developed here—where swinging, stopping, and spinning share a unified spectral structure—does it become possible to identify the stopping regime as the common continuum limit of the swinging and spinning spectra.

## V. THEORETICAL METHOD

For  $k > 1$ , the elliptic integral and its argument may become complex; nevertheless, both  $\kappa$  and  $\Re[K(k)]$  remain well-defined positive real quantities. For numerical implementation, it is often convenient to use standard transformation properties of  $K$ , yielding:

$$\begin{aligned}
k < 1 : \quad \kappa &= K(\sqrt{1 - k^2}), & T &= \frac{4K(k)}{\Omega_L} \\
k = 1 : \quad \kappa &= \frac{\pi}{2}, & T &\rightarrow \infty \\
k > 1 : \quad \kappa &= \frac{1}{k}K(\sqrt{1 - 1/k^2}), & T &= \frac{4K(1/k)}{k\Omega_L}
\end{aligned} \tag{18}$$

The technical proofs of the exact frequency-domain solutions are provided in Supplementary Material. Here we summarize the guiding principles: the unified frequency-domain structure becomes transparent only after three key perspective shifts.

1. *Choice of initial condition.* Instead of adopting the traditional formulation in which the pendulum is released from rest at an amplitude  $\phi_0$ , we consider the motion initiated at the bottom. This perspective naturally promotes the initial angular speed  $\omega_m$  to a characteristic parameter, enabling continuous transitions between all three classes of motion.
2. *Choice of dynamical variable.* The challenge in finding the exact Fourier coefficients arises from the fact that the Jacobi elliptic function is embedded within the arcsin function. However, we have found that the  $\arcsin[\dots]$  dependence of  $\phi(t)$  can be avoided if one initially focuses on the angular velocity  $\omega(t)$ . Once its spectral content is obtained, one gains access to the frequency-domain solution of  $\phi(t)$  via simple integration.
3. *Choice of period in the spinning regime.* The motion can be decomposed exactly into a linear phase drift plus a periodic phase oscillation. The oscillatory component remains strictly periodic. Exploiting this periodicity, we adopt twice the primitive oscillation period as the fundamental period—an admissible spectral choice—which aligns the harmonic lattice of the spinning solution with that of the swinging solution. This step is not merely technical: it reveals that both regimes share an identical analytic coefficient structure and differ only by parity selection. It also permits the separatrix to be identified as the continuum limit common to both regimes.

Together, each perspective shift reveals the solution layer by layer—(i) disentangling regime classification, (ii) removing the arcsin obstruction, and (iii) exposing parity and the continuum limit—thereby unifying the exact spectral structure across all regimes of motion.

## A. Identical Spectral Structure

At first glance, the continuum coefficient  $C(\Omega)$  appears to differ from the discrete harmonic coefficient  $c_n$  by a factor of two. However,  $c_n$  represents a discrete harmonic amplitude, whereas  $C(\Omega)$  is a spectral density in frequency space. A direct comparison is:

$$c_n \longleftrightarrow C(\Omega) \Delta\Omega. \quad (19)$$

Near the separatrix, where the harmonic spacing collapses, the discrete lattice satisfies  $\Delta\Omega = 2\Omega_0$  due to parity selection. The effective discrete amplitude is therefore  $C(\Omega) \Delta\Omega$ , which restores the same analytic coefficient structure as  $c_n$ .

The factor of two in  $C(\Omega)$  is thus not a deviation from unification, but the precise normalization factor required to preserve it.

## B. Derivation via Spectral Discretization

Because all regimes share an identical spectral structure, the exact frequency-domain solutions can be derived without invoking Jacobi elliptic functions or their known Fourier series. Starting from the separatrix, the equation of motion reduces to a first-order ODE in  $\omega = \dot{\phi}$ , yielding directly the continuous spectral representation

$$\text{separatrix: } \phi(t) = \int_0^\infty \frac{2}{\Omega \cosh\left(\frac{\pi}{2} \frac{\Omega}{\Omega_L}\right)} \sin(\Omega t) d\Omega. \quad (20)$$

Identifying  $\pi/2$  as the limiting value of the imaginary period  $\kappa = K(\sqrt{1-k^2})$  as  $k \rightarrow 1$  naturally connects the separatrix to the periodic regimes via spectral discretization—that is, a sampling of the same underlying spectral kernel determined by the distance to the nearest singularity in the complex time plane. Recognizing that the swinging and spinning motions correspond to discrete samplings of this kernel, one recovers precisely the frequency-domain solutions in Eq. (3) and Eq. (6).

The frequency-domain formulation presented here therefore provides simultaneous access to three complementary aspects of pendulum-like dynamics:

1. *Time-domain behavior*—obtained by summing the harmonic components, reproducing the exact trajectories traditionally expressed through Jacobi-type solutions.

2. *Frequency-domain structure*—revealed explicitly through the closed-form spectral kernel, which remains implicit in the conventional time-domain formulation and typically requires perturbative or numerical extraction.
3. *Regime symmetry and transition*—clarified through odd/even harmonic selection and the discrete-to-continuum limit connecting oscillatory, separatrix, and rotational motions.

Thus, rather than presenting a mere alternative reframing of the classical solution, this work reveals the analytic and spectral geometry underlying pendulum-like systems, from which all dynamical regimes emerge naturally through symmetry selection and spectral discretization.

## VI. CONCLUSION

We have presented a complete and exact frequency-domain formulation of energy-conserving pendulum-like dynamics that unifies swinging, stopping, and spinning motions within a single analytic framework. By exposing the spectral structure common to all regimes, this approach reveals that qualitative changes in motion arise not from altered frequency scales or deformed spectra, but from systematic reorganizations of spectral weight—through parity selection and, at the separatrix, through a dynamical collapse of the fundamental frequency. These results resolve a long-standing gap in the frequency-domain description of the nonlinear pendulum and provide a transparent interpretation of regime transitions that has remained inaccessible in conventional time-domain treatments.

## ACKNOWLEDGMENTS

The author thanks the Potjanachaisak family for their hospitality during a summer research visit in Chiang Khrua, Sakon Nakhon Province, Thailand.

## AUTHOR DECLARATIONS

### Conflict of Interest

The authors have no conflicts to disclose.

## DATA AVAILABILITY

All data and code necessary to reproduce the results in this work are publicly available at <https://github.com/teepanis/nonlinear-pendulum>.

## REFERENCES

- <sup>1</sup>G. M. Moatimid and T. S. Amer, “Analytical solution for the motion of a pendulum with rolling wheel: stability analysis,” *Scientific Reports* **12**, 12628 (2022).
- <sup>2</sup>P. F. Hinrichsen, “Nonlinear oscillator acceleration and period variation with amplitude,” *American Journal of Physics* **91**, 979–987 (2023).
- <sup>3</sup>P. F. Hinrichsen, “Rectangular compound pendulums,” *The Physics Teacher* **61**, 572–575 (2023).
- <sup>4</sup>S. Zhang, “Nonlinear analysis of compound pendulum model,” *Physica Scripta* **99**, 115271 (2024).
- <sup>5</sup>S. V. Kontomaris, I. Mazi, G. Chliveros, and A. Malamou, “Generic numerical and analytical methods for solving nonlinear oscillators,” *Physica Scripta* **99**, 025231 (2024).
- <sup>6</sup>A. H. MacDonald and M. Plischke, “Study of the driven damped pendulum: Application to josephson junctions and charge-density-wave systems,” *Physical Review B* **27**, 201–211 (1983).
- <sup>7</sup>P. Mangin and R. Kahn, *Superconductivity: An introduction* (Springer International Publishing, 2016).
- <sup>8</sup>I. Marino, S. Raghavan, S. Fantoni, S. R. Shenoy, and A. Smerzi, “Bose-condensate tunneling dynamics: Momentum-shortened pendulum with damping,” *Physical Review A* **60**, 487–493 (1999).
- <sup>9</sup>M. Pigneur and J. Schmiedmayer, “Analytical pendulum model for a bosonic josephson junction,” *Physical Review A* **98**, 063632 (2018).

- <sup>10</sup>M. Marszal, B. Witkowski, K. Jankowski, P. Perlikowski, and T. Kapitaniak, “Energy harvesting from pendulum oscillations,” *International Journal of Non-Linear Mechanics* **94**, 251–256 (2017).
- <sup>11</sup>H. Fu, J. Jiang, S. Hu, J. Rao, and S. Theodossiades, “A multi-stable ultra-low frequency energy harvester using a nonlinear pendulum and piezoelectric transduction for self-powered sensing,” *Mechanical Systems and Signal Processing* **189**, 110034 (2023).
- <sup>12</sup>W. Feng, H. Chen, Q. Zou, D. Wang, X. Luo, C. Cummins, C. Zhang, S. Yang, and Y. Su, “A contactless coupled pendulum and piezoelectric wave energy harvester: Model and experiment,” *Energies* **17**, 876 (2024).
- <sup>13</sup>A. S. Krishnapriyan, A. F. Queiruga, N. B. Erichson, and M. W. Mahoney, “Learning continuous models for continuous physics,” *Communications Physics* **6**, 319 (2023).
- <sup>14</sup>J. Marion and S. Thornton, *Classical Dynamics of Particles and Systems* (Saunders College Pub., 1995).
- <sup>15</sup>T. Kibble and F. Berkshire, *Classical Mechanics (5th Edition)* (World Scientific Publishing Company, 2004).
- <sup>16</sup>J. Taylor, *Classical Mechanics* (University Science Books, 2004).
- <sup>17</sup>T. E. Roth, R. Ma, and W. C. Chew, “The transmon qubit for electromagnetics engineers: An introduction,” *IEEE Antennas and Propagation Magazine* **65**, 8–20 (2023).
- <sup>18</sup>M. R. Matthews, C. Gauld, and A. Stinner, “The pendulum: Its place in science, culture and pedagogy,” *Science & Education* **13**, 261–277 (2004).
- <sup>19</sup>A. Beléndez, C. Pascual, D. Méndez, T. Beléndez, and C. Neipp, “Exact solution for the nonlinear pendulum,” *Revista Brasileira de Ensino de Física* **29**, 645–648 (2007).
- <sup>20</sup>K. Ochs, “A comprehensive analytical solution of the nonlinear pendulum,” *European Journal of Physics* **32**, 479–490 (2011).
- <sup>21</sup>DLMF, “*NIST Digital Library of Mathematical Functions*,” <https://dlmf.nist.gov/>, Release 1.2.4 of 2025-03-15, f. W. J. Olver, A. B. Olde Daalhuis, D. W. Lozier, B. I. Schneider, R. F. Boisvert, C. W. Clark, B. R. Miller, B. V. Saunders, H. S. Cohl, and M. A. McClain, eds.
- <sup>22</sup>F. M. Lima, “Simple but accurate periodic solutions for the nonlinear pendulum equation,” *Revista Brasileira de Ensino de Física* **41** (2018), 10.1590/1806-9126-rbef-2018-0202.
- <sup>23</sup>I. Singh, P. Arun, and F. Lima, “Fourier analysis of nonlinear pendulum oscillations,” *Revista Brasileira de Ensino de Física* **40** (2018), 10.1590/1806-9126-rbef-2017-0151.

- <sup>24</sup>R. Simon and R. P. Riesz, “Large amplitude simple pendulum: A fourier analysis,” *American Journal of Physics* **47**, 898–899 (1979).
- <sup>25</sup>A. Beléndez, E. Arribas, M. Ortuño, S. Gallego, A. Márquez, and I. Pascual, “Approximate solutions for the nonlinear pendulum equation using a rational harmonic representation,” *Computers & Mathematics with Applications* **64**, 1602–1611 (2012).
- <sup>26</sup>K. Johannessen, “An anharmonic solution to the equation of motion for the simple pendulum,” *European Journal of Physics* **32**, 407–417 (2011).
- <sup>27</sup>V. Méndez, C. Sans, D. Campos, and I. Llopis, “Fourier series expansion for nonlinear hamiltonian oscillators,” *Physical Review E* **81**, 066201 (2010).
- <sup>28</sup>S. Gil, A. E. Legarreta, and D. E. D. Gregorio, “Measuring anharmonicity in a large amplitude pendulum,” *American Journal of Physics* **76**, 843–847 (2008).
- <sup>29</sup>P. F. Hinrichsen, “Fourier analysis of the non-linear pendulum,” *American Journal of Physics* **88**, 1068–1074 (2020).
- <sup>30</sup>L. P. Fulcher and B. F. Davis, “Theoretical and experimental study of the motion of the simple pendulum,” *American Journal of Physics* **44**, 51–55 (1976).
- <sup>31</sup>S. C. Zilio, “Measurement and analysis of large-angle pendulum motion,” *American Journal of Physics* **50**, 450–452 (1982).
- <sup>32</sup>T. Chachiyo, “Simple and accurate complete elliptic integrals for the full range of modulus,” *Computer Physics Communications* **319**, 109931 (2026).
- <sup>33</sup>S. Rasmussen, K. Christensen, S. Pedersen, L. Kristensen, T. Bækkegaard, N. Loft, and N. Zinner, “Superconducting circuit companion—an introduction with worked examples,” *PRX Quantum* **2**, 040204 (2021).
- <sup>34</sup>A. Shnirman, G. Schön, and Z. Hermon, “Quantum manipulations of small josephson junctions,” *Physical Review Letters* **79**, 2371–2374 (1997).
- <sup>35</sup>S. Kim, L. V. Abdurakhimov, D. Pham, W. Qiu, H. Terai, S. Ashhab, S. Saito, T. Yamashita, and K. Semba, “Superconducting flux qubit with ferromagnetic josephson  $\pi$ -junction operating at zero magnetic field,” *Communications Materials* **5**, 216 (2024).
- <sup>36</sup>M. AbuGhanem, “IBM quantum computers: evolution, performance, and future directions,” *The Journal of Supercomputing* **81**, 687 (2025).
- <sup>37</sup>F. Arute, K. Arya, R. Babbush, D. Bacon, J. C. Bardin, R. Barends, R. Biswas, S. Boixo, F. G. S. L. Brandao, D. A. Buell, B. Burkett, Y. Chen, Z. Chen, B. Chiaro, R. Collins, W. Courtney, A. Dunsworth, E. Farhi, B. Foxen, A. Fowler, C. Gidney, M. Giustina,

- R. Graff, K. Guerin, S. Habegger, M. P. Harrigan, M. J. Hartmann, A. Ho, M. Hoffmann, T. Huang, T. S. Humble, S. V. Isakov, E. Jeffrey, Z. Jiang, D. Kafri, K. Kechedzhi, J. Kelly, P. V. Klimov, S. Knysh, A. Korotkov, F. Kostritsa, D. Landhuis, M. Lindmark, E. Lucero, D. Lyakh, S. Mandrà, J. R. McClean, M. McEwen, A. Megrant, X. Mi, K. Michielsen, M. Mohseni, J. Mutus, O. Naaman, M. Neeley, C. Neill, M. Y. Niu, E. Ostby, A. Petukhov, J. C. Platt, C. Quintana, E. G. Rieffel, P. Roushan, N. C. Rubin, D. Sank, K. J. Satzinger, V. Smelyanskiy, K. J. Sung, M. D. Trevithick, A. Vainsencher, B. Villalonga, T. White, Z. J. Yao, P. Yeh, A. Zalcman, H. Neven, and J. M. Martinis, “Quantum supremacy using a programmable superconducting processor,” *Nature* **574**, 505–510 (2019).
- <sup>38</sup>D. Gao, D. Fan, C. Zha, J. Bei, G. Cai, J. Cai, S. Cao, F. Chen, J. Chen, K. Chen, X. Chen, X. Chen, Z. Chen, Z. Chen, Z. Chen, W. Chu, H. Deng, Z. Deng, P. Ding, X. Ding, Z. Ding, S. Dong, Y. Dong, B. Fan, Y. Fu, S. Gao, L. Ge, M. Gong, J. Gui, C. Guo, S. Guo, X. Guo, L. Han, T. He, L. Hong, Y. Hu, H.-L. Huang, Y.-H. Huo, T. Jiang, Z. Jiang, H. Jin, Y. Leng, D. Li, D. Li, F. Li, J. Li, J. Li, J. Li, J. Li, N. Li, S. Li, W. Li, Y. Li, Y. Li, F. Liang, X. Liang, N. Liao, J. Lin, W. Lin, D. Liu, H. Liu, M. Liu, X. Liu, X. Liu, Y. Liu, H. Lou, Y. Ma, L. Meng, H. Mou, K. Nan, B. Nie, M. Nie, J. Ning, L. Niu, W. Peng, H. Qian, H. Rong, T. Rong, H. Shen, Q. Shen, H. Su, F. Su, C. Sun, L. Sun, T. Sun, Y. Sun, Y. Tan, J. Tan, L. Tang, W. Tu, C. Wan, J. Wang, B. Wang, C. Wang, C. Wang, C. Wang, J. Wang, L. Wang, R. Wang, S. Wang, X. Wang, X. Wang, X. Wang, Y. Wang, Z. Wei, J. Wei, D. Wu, G. Wu, J. Wu, S. Wu, Y. Wu, S. Xie, L. Xin, Y. Xu, C. Xue, K. Yan, W. Yang, X. Yang, Y. Yang, Y. Ye, Z. Ye, C. Ying, J. Yu, Q. Yu, W. Yu, X. Zeng, S. Zhan, F. Zhang, H. Zhang, K. Zhang, P. Zhang, W. Zhang, Y. Zhang, Y. Zhang, L. Zhang, G. Zhao, P. Zhao, X. Zhao, X. Zhao, Y. Zhao, Z. Zhao, L. Zheng, F. Zhou, L. Zhou, N. Zhou, N. Zhou, S. Zhou, S. Zhou, Z. Zhou, C. Zhu, Q. Zhu, G. Zou, H. Zou, Q. Zhang, C.-Y. Lu, C.-Z. Peng, X. Zhu, and J.-W. Pan, “Establishing a new benchmark in quantum computational advantage with 105-qubit zuchongzhi 3.0 processor,” *Physical Review Letters* **134**, 090601 (2025).
- <sup>39</sup>J. Bardeen, L. N. Cooper, and J. R. Schrieffer, “Theory of superconductivity,” *Physical Review* **108**, 1175–1204 (1957).
- <sup>40</sup>J. A. Blackburn, M. Cirillo, and N. Grønbech-Jensen, “A survey of classical and quantum interpretations of experiments on josephson junctions at very low temperatures,” *Physics Reports* **611**, 1–33 (2016).

- <sup>41</sup>A. Smerzi, S. Fantoni, S. Giovanazzi, and S. R. Shenoy, “Quantum coherent atomic tunneling between two trapped bose-einstein condensates,” *Physical Review Letters* **79**, 4950–4953 (1997).
- <sup>42</sup>G. J. Milburn, J. Corney, E. M. Wright, and D. F. Walls, “Quantum dynamics of an atomic bose-einstein condensate in a double-well potential,” *Physical Review A* **55**, 4318–4324 (1997).
- <sup>43</sup>M. Albiez, R. Gati, J. Fölling, S. Hunsmann, M. Cristiani, and M. K. Oberthaler, “Direct observation of tunneling and nonlinear self-trapping in a single bosonic josephson junction,” *Physical Review Letters* **95**, 010402 (2005).
- <sup>44</sup>L. J. LeBlanc, A. B. Bardou, J. McKeever, M. H. T. Extavour, D. Jervis, J. H. Thywissen, F. Piazza, and A. Smerzi, “Dynamics of a tunable superfluid junction,” *Physical Review Letters* **106**, 025302 (2011).